Calculations of current densities and aromatic pathways in cyclic porphyrin and isoporphyrin arrays

Franzke, Yannick J.

2017-05-28

Franzke , Y J , Sundholm , D & Weigendb , F 2017 , ' Calculations of current densities and aromatic pathways in cyclic porphyrin and isoporphyrin arrays ' , Physical Chemistry Chemical Physics , vol. 19 , no. 20 , pp. 12794-12803 . https://doi.org/10.1039/c7cp00624a

http://hdl.handle.net/10138/309506
https://doi.org/10.1039/c7cp00624a

unspecified
acceptedVersion

Journal Name

ARTICLE TYPE

Cite this: DOI: 10.1039/xxxxxxxxxx

Calculations of current densities and aromatic pathways in cyclic porphyrin and isoporphyrin arrays†

Yannick J. Franzke,[a,b] Dage Sundholm*[a] and Florian Weigend[b,c]

Received Date
Accepted Date

DOI: 10.1039/xxxxxxxxxx

www.rsc.org/journalname

Magnetically induced current density susceptibilities have been studied for a number of cyclic ethyne- and butadiyne-bridged porphyrin and isoporphyrin arrays. The current density susceptibilities have been calculated using the gauge-including magnetically induced current (GIMIC) method, which is interfaced to the TURBOMOLE quantum chemistry code. Aromatic properties and current pathways have been analyzed and discussed by numerical integration of the current density susceptibilities passing selected chemical bonds yielding current strength susceptibilities. Despite the interrupted π-framework, zinc(II) isoporphyrin sustains a ring current of ca. 10 nA/T. Porphyrin and isoporphyrin dimers sustain a significant current strength at the linker, whereas the larger porphyrinoid arrays sustain mainly local ring currents. Isoporphyrin dimers with saturated meso carbons have strong net diatropic ring-current strengths of 20 nA/T fulfilling Hückels aromaticity rule. Porphyrin trimers and tetramers exhibit almost no current strength at the linker. The porphyrin moieties maintain their strong net diatropic ring current.

1 Introduction

Porphyrin and porphyrinoids form the basis of many important biochemical compounds. The most prominent example might be the green color pigment chlorophyll in plants. Porphyrin shows a versatile chemistry due to its aromaticity and rich coordination chemistry, which has resulted in numerous applications such as nonlinear optical materials, near-infra-red dyes, photovoltaic dyes and their use in photomedical and biomedical applications in cancer treatment.[1–12] Conjugated multiporphyrins allowing for fine-tuning of electronic, optical and magnetic properties have been recently reviewed.[13] Cyclic multiporphyrin arrays can be prepared via metal-catalyzed cross-coupling reactions.[14–17]

Free-base isoporphyrin is a tautomeric form of free-base porphyrin. Compared to porphyrin, little is known about the chemical and physical properties of isoporphyrin. In isoporphyrin, one hydrogen of the NH groups is formally moved to a meso-carbon atom. Free-base isoporphyrin shows a tendency to undergo back tautomerization to porphyrin re-establishing the strong aromatic system. The first metalloisoporpyrin was synthesized by Dolphin *et al.* nearly 50 years ago.[18] The structure of the prepared zinc(II) tetraarylisoporphyrin was examined by NMR spectroscopy. The β protons of the isoporphyrin ring exhibit an upshift of about 2 ppm. An analogous behavior has been observed for zinc phlorins,[19] which was explained by the lack of a ring current due to the saturated meso-carbon atom.[18,19] Crystallographic, electrochemical and spectroscopic characterizations of zinc(II) isoporphyrin salts prepared as chromophores have been done by Fajer *et al.*[20–22] As expected, the interrupted π-system causes the bond lengths to alternate. Nowadays, isoporphyrin is proposed to be an intermediate in heme oxygenase catalysis.[23,24] Various synthetic routes have been developed during the last 15 years.[25–30] Current trends and potential applications as photosensitizers in biomedical research and near infra-red dyes have been reviewed

[a] *Department of Chemistry, University of Helsinki, P.O.Box 55, FIN-00014 Helsinki, Finland; E-mail: Dage.Sundholm@helsinki.fi*
[b] *Institute of Physical Chemistry, Karlsruhe Institute of Technology, Kaiserstr. 12, 76131 Karlsruhe, Germany*
[c] *Institute of Nanotechnology, Karlsruhe Institute of Technology, Hermann-von-Helmholtz-Platz 1, 76344 Karlsruhe, Germany*

† Electronic Supplementary Information (ESI) available: Cartesian coordinates of the optimized structures and NMR shielding constants. Additional streamline plots and current pathways. See DOI: 10.1039/b000000x/

lately.[31]

The aim of this work is to provide insight into current and electron delocalization pathways in cyclic ethyne- and butadiyne-bridged multiporphyrin and isoporphyrin arrays. In addition to the porphyrin rings, the porphyrinoid arrays feature an inner ring established by the sp-hybridized linkers. To the best of our knowledge, such isoporphyrin oligomers have not yet been prepared. Two different linkers have been chosen in order to vary the number of electrons for assessing whether Hückel's aromaticity rule is fullfilled.[32–35] Electron delocalization cannot be easily observed experimentally. Thus, computational studies are needed for providing a deeper insight and may be helpful in the design of new porphyrin-based materials. Accurate magnetically induced current density susceptibilities and current strength susceptibilities are obtained by using the gauge-including magnetically induced current (GIMIC) method.[36–39] GIMIC has proven to be a useful tool for assigning the aromaticity of porphyrinoids.[40–49] Reliable current pathways can be obtained in multiring systems, for which other approaches may fail.[50–60] GIMIC studies have shown that the 18 π [18]annulene pathway postulated for porphyrinoids is an oversimplification and that all 26 π-electrons are part of the current pathway. The previous studies are here extended to account for cyclic multiring porphyrinoid systems.

The article is structured as follows. The computational methods and the corresponding optimized structures are presented in Sections 2 and 3. The results of the current density and strength calculations are analyzed and discussed in Section 4. The main results are summarized in Section 5, where the conclusions are drawn.

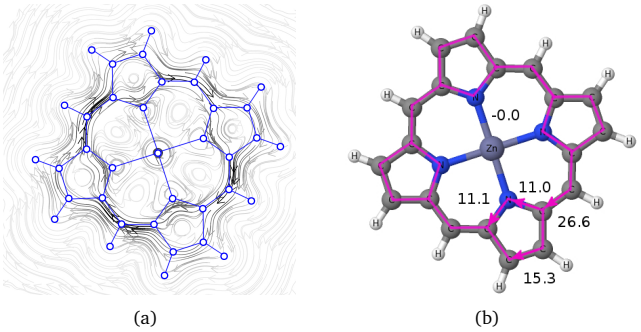

(a) (b)

Fig. 1 (a) Streamline plot of the calculated magnetically induced current densities calculated 1 bohr above the molecular plane of ZnP (**1**). (b) Calculated net current strengths passing selected bonds are given for ZnP (**1**). The current pathway is drawn in pink. Arrows are drawn for absolute values of current strengths greater than 0.5 nA/T.

2 Computational Methods

The molecular structures were optimized at the density functional theory (DFT) level using Becke's three parameter functional combined with the Lee-Yang-Parr exchange-correlation functional (B3LYP)[61,62] as implemented in TURBOMOLE Version 7.0 and Version 7.1.[63–65] The Karlsruhe triple-ζ basis set augmented with polarization functions (def2-TZVP) and grid size m5 were used for all atoms.[66,67] The NMR shielding calculations were performed at the DFT/B3LYP level of theory using a split-valence polarization basis set (def2-SVP)[66,67] and the MPSHIFT module of TURBOMOLE.[68–70] The dispersion correction D3 was employed in the structure optimization procedures.[71] Substituents present in the synthesized structures were omitted to save computational time.

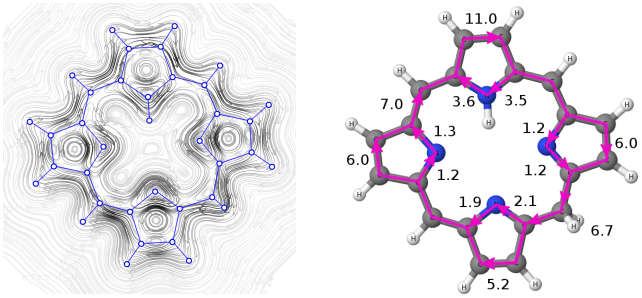

(a) (b)

Fig. 2 (a) Streamline plot of the calculated magnetically induced current densities calculated 1 bohr above the molecular plane of IP (**2**). (b) Calculated net current strengths passing selected bonds are given for IP (**2**). The current pathway is drawn in pink.

Current-density susceptibilities and current-strength susceptibilities were calculated at the B3LYP/def2-SVP level with GIMIC.[36–39] We use the shorter terms current density and current strength in the rest of the article. GIMIC is an independent program that requires the atomic orbital density matrices and the corresponding first-order magnetically perturbed density matrices from the NMR shielding calculations. Gauge-including atomic orbitals (GIAOs) are employed resulting in gauge-origin independence of the current densities and a fast basis set convergence.[36] The magnetic field was oriented perpendicularly to the molecular plane. The direction of the magnetic field was chosen so that diatropic ring currents circle in the clockwise direction and paratropic ring currents in the anticlockwise direction. The current densities were analyzed by calculating current pathways, which are determined by numerical integration of the magnetically induced current densities yielding current strengths (in nA/T). Integration of the current density was performed on a plane perpendicularly to the molecular plane and parallel to the applied magnetic field.

The Figures were made using Jmol[72] and GIMP.[73] A positive sign or an arrow in the clockwise direction indicates a net diatropic current and negative signs or arrows in the anticlockwise direction mark net paratropic current strengths. Arrows are usually drawn for current pathways whose absolute value of the current

strength is greater than 0.5 nA/T.

3 Molecular Structures and Nomenclature

To elucidate general trends regarding the aromaticity and current pathways in multiporphyrinoid arrays, we constructed cyclic dimers, trimers and tetramers of porphyrinoids. The number of available valence electrons was adjusted by using ethyne and butadiyne bridges connecting the porphyrinoid rings. We use the abbreviations ZnP for zinc(II) porphyrin and ZnIP for the zinc(II) isoporphyrin cation. The Cartesian coordinates of all optimized structures are given in the ESI†. The porphyrin framework of the optimized structures is planar. The structure, magnetically induced densities and the current pathway of the ZnP monomer are shown in Fig. 1. The current strengths of ZnP serve as reference for the oligomers. The optimized structure of free-base isoporphyrin (IP) is shown in Fig. 2. IP exhibits C–C bond lengths of 1.49 Å at the saturated meso carbon, which are in the expected region for single C–C bonds.[74] The H-C_{meso}-H bond angle is 103.1°. Thus, the sp^3 hybridized meso carbon forms a slightly distorted tetrahedron. The structural parameters of the ZnIP cation in Fig. 3 are very similar. The IP monomer and oligomers have one hydrogen atom inside each of the isoporphyrin rings. Hydrogen migration that has been studied extensively in free-base porphyrinoids using experimental and theoretical methods[75–86] is likely to occur in free-base isoporphyrin as well. Therefore, we consider only one constitutional isomer of the free-base isoporphyrin oligomers in this work. The dimers are obtained by connecting two porphyrin or isoporphyrin rings with two ethyne or butadiyne linkers at the β positions. The ethyne-bridged ZnP dimer is shown in Fig. 4. The ZnIP dimer possessing a net charge of +2 is displayed in Fig. 5 and the neutral IP dimer is shown in Fig. 6.

The current pathways of the neutral ZnP dimers with saturated meso-carbon atoms (ZnPS) have also been studied. These compounds form an intermediate between the ZnP and ZnIP dimers. The ethyne-bridged ZnPS dimer is depicted in Fig. 7. Only the ZnPS dimer is studied to maintain a closed-shell configuration, because the neutral ZnPS monomer is an open-shell species. The butadiyne-bridged ZnP trimer is shown in Fig. 8. The butadiyne linkers of the ZnP and IP trimers and tetramers can be placed at the β or meso position. The β-carbon linked ZnP tetramer is shown in Fig. 9. The increasing structural distortion of the β-carbon bridged compounds is seen in the figures. We have studied only free-base butadiyne-bridged IP tetramers to avoid IP compounds with high charges. The free-base β-carbon bridged IP tetramer is shown in Fig. 10.

3.1 Hückel's aromaticity rule

The aromaticity of annelated hydrocarbon rings can be understood by employing Hückel's aromaticity rule, even though the rule was originally intended for planar annulenes and other

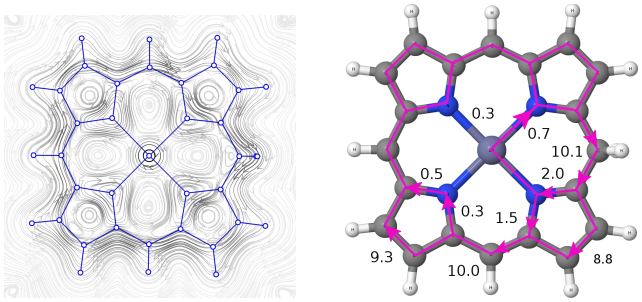

(a) (b)

Fig. 3 (a) Streamline plot of the calculated magnetically induced current densities calculated 1 bohr above the molecular plane of ZnIP (**3**). (b) Calculated net current strengths passing selected bonds are given for ZnIP (**3**). The current pathway is drawn in pink.

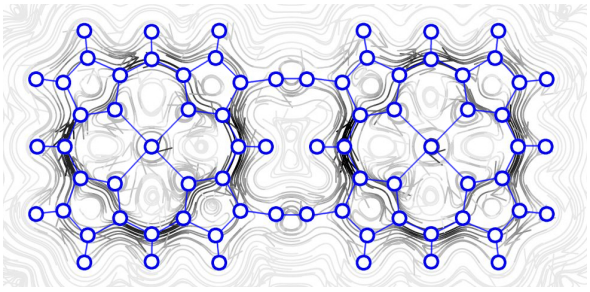

(a)

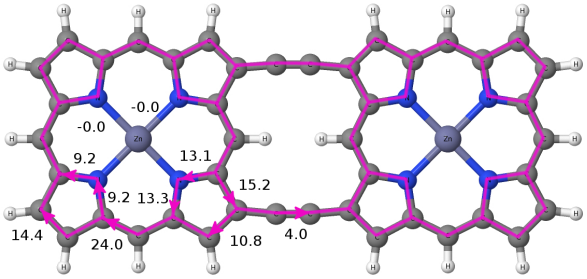

(b)

Fig. 4 (a) Streamline plot of the calculated magnetically induced current densities calculated 1 bohr above the molecular plane of a ethyne-bridged ZnP dimer (**5**). (b) Calculated net current strengths passing selected bonds are given for an ethyne-bridged ZnP dimer (**5**). The current pathway is drawn in pink. A net paratropic current strength is found along the linker.

molecules that can be approximated using the particle-in-a-ring or particle-on-a-circular-disk models.[32–35,87,88] Thus, the Hückel rule of aromaticity is a symmetry property. Current density calculations have shown that Hückel's rule can be used for understanding aromatic properties of large ring-shaped hydrocarbons consisting of several coupled and annelated rings.[89] For molecules

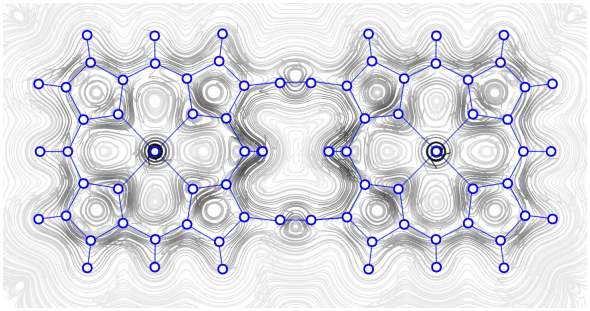

(a)

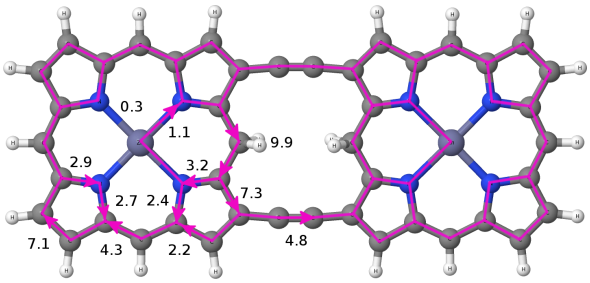

(b)

Fig. 5 (a) Streamline plot of the calculated magnetically induced current densities calculated 1 bohr above the molecular plane of the dicationic ethyne-bridged ZnIP dimer (12). (b) Calculated net current strengths passing selected bonds are given for the ethyne-bridged ZnIP dimer (12). The current pathway is drawn in pink. The net current strength through the linker is paratropic.

consisting of several annelated formally aromatic rings, the actual current flow determines the aromatic nature of the molecule. When several current pathways are possible, the current pathway is determined by the energetic stability of the local and global aromaticity of the molecule. Thus, local aromaticity may be in conflict with the global one and *vice versa*; the energetically most favourable situation wins.

Current density calculations on porphyrins showed that the aromatic properties are not properly described by the traditional 18 π annulene model, because all its 26 π- electrons contribute to the aromatic pathway.[42] The aromaticity of porphyrins and annulenes have also been interpreted based on orbital contributions to the current density,[90–92] even though electrons according to quantum mechanics are indistinguishable. The Hückel rule has been extended to nonplanar and twisted molecules.[93,94] A generalisation of the Hückel's rule is used for understanding the aromaticity of Möbius twisted molecules.[40,41,93,95–100] However, Hückel's rule often fails to describe the aromaticity of molecules consisting of annelated aromatic and antiaromatic rings.[101,102] Explicit calculations of the current pathway are then needed for understanding the aromatic pathway of complicated molecules like tropiporphyrin.[49]

In this work, we compare the aromatic character of the porphyrinoid arrays obtained using Hückel's rule with the ones deduced from calculated current densities. The individual ZnP and ZnIP moieties have 26 π-electrons and 24 π-electrons, respectively, whereas each ZnPS unit contributes with 25 π-electrons. The ethyne and butadiyne bridges contribute each with 2 π- and 4 π-electrons, respectively.

The porphyrinoid dimers consist of three annelated rings namely the two porphyrinoids and the ring between them. The external magnetic field can induce diatropic ring currents around the porphyrins, which leads either to a paratropic ring current in the middle ring or alternatively no current passes the bridge between the porphyrins. The ring current of the porphyrinoids can fork into a local ring current around the porphyrinoid and a part of the current flow forms a global current around the whole molecule. Another possibility is that the ring in the middle is strongly aromatic and the porphyrinoids are nonaromatic, which is unlikely, because the aromatic stabilisation energy of the porphyrinoids is then lost. The same approach can be used for understanding the aromatic character of the trimers and tetramers.

4 Results and Discussion

To visualize the motion of electrons in molecular systems in the presence of an external magnetic field, streamline plots of the magnetically induced current densities calculated in a plane placed 1 bohr above the molecular plane and current pathways obtained by numerical integration of the current densities passing chemical bonds or atoms are given in Fig. 1-10. The streamline plots allow for a qualitative understanding of current flows and current strengths can be used to quantify the degree of aromaticity. A threshold criterion of 0.5 nA/T is applied to establish the pathways. The calculated chemical shifts are given in the ESI†. Additional streamline representations and current pathways of discussed molecules are shown in the ESI†. The current pathway of the aromatic ZnP (Fig. 1) serves as a reference to all other molecules. Despite the interrupted π-system, all isoporphyrin units sustain a non-negligible current strength through the saturated meso-carbon atom. The dimers exhibit significant current strengths passing the bonds of the linker. According to the magnetic criterion for aromaticity, the ZnP and ZnIP dimers are antiaromatic, whereas the ZnPS dimers are aromatic. The ZnP trimer as well as the ZnP and IP tetramers widely maintain the current pathways and current strengths of isolated porphyrinoids without any significant global net current flow.

4.1 Free-Base Isoporphyrin and Zinc Isoporphyrin

Free-base isoporphyrin (**2**) is about 178 kJ/mol higher in energy than free-base porphyrin (**1**) at the employed computational level. The streamline plot and the current pathway in Fig. 2 show

no interruption of the current flow at the saturated meso-carbon atom. A net diatropic current strength of 6.7-7.0 nA/T is found to flow around the ring. This is consistent with the calculated chemical shifts of 7-8 ppm for the protons at the β carbons. A similar behavior has been observed for cyclopentadiene, which has a current strength of 5.4-5.6 nA/T through the saturated CH_2 group,[103,104] which can be compared with the ring-current strength of 11.8 nA/T for benzene at the same level of theory.[104] Thus, free-base isoporphyrin is aromatic judged from the ring-current criterion but it is not as aromatic as free-base porphyrin.

The current pathway of IP splits at each pyrrole ring into an inner C-N and an outer all carbon route. The outer route is preferred with current strengths of 5.2-6.0 nA/T as compared to 1.2-1.3 and 1.9-2.1 nA/T for the inner one. A local diatropic ring current of 3.5-3.6 nA/T is sustained by the pyrrole ring with the NH moiety.

For ZnIP (**3**), the current strength through the CH_2 group of 10.1 nA/T is somewhat stronger than for free-base IP. A streamline plot of the current density and the current pathway are shown in Fig. 3. The pathway splits at the pyrrolic units into a C-N route and a strongly favored outer all carbon route. At the pyrrole ring next to the CH_2 group a current of 8.8 nA/T take the outer route and 1.5-2.0 nA/T passes along the inner route. The Zn-N-C six-membered ring containing the saturated meso carbon sustains a weak local diatropic ring current of 0.7 nA/T. At the other pyrrole unit only 0.3-0.5 nA/T passes through the inner C_α-N bond and 9.3 nA/T through the C_β-C_β bond. ZnP does not have any classically forbidden radial currents.

Even a free-base isoporphyrin with two saturated meso-carbon atoms (**4**) shows a current strength of 11.0 nA/T through the CH_2 moiety.

4.2 Zinc Porphyrin Dimers

Magnetically induced current densities and current pathways were calculated for the ethyne- and butadiyne-bridged ZnP dimers (**5**) and (**6**). The streamline representation of the current densities and the current pathway of the ethyne-bridged ZnP dimer are shown in Fig. 4. The chemical shifts of the outer hydrogen atoms are close to 10 ppm and the chemical shift of the hydrogens inside the ring formed by the ethyne bridges and the porphyrins is 15.5 ppm. A paratropic current flow reigns inside that inner ring and a diatropic current flow is predominant outside it. Thus, the local diatropic current flow of the porphyrin and the inner ring are in the same direction strongly deshielding the inner hydrogens. However, the chemical shift does not indicate whether a significant net current flow through the linker exists. A net current strength of 28.3 nA/T is obtained in the common bonds of the porphyrin and the inner ring. The current forks into a current of 13.1 nA/T that passes via N and 15.2 nA/T continues to the α carbon, where it splits into a current of 10.9 nA/T along the C_α-C_α bond and a current of -4.0 nA/T that passes along the ethyne bridge to the other porphyrin unit. The current across the ethyne bridge is locally paratropic indicating antiaromaticity of the inner ring. The current of 24.0 nA/T flowing around the porphyrin ring splits into an inner current of 9.2 nA/T and 14.4 nA/T takes the outer route.

The current pathways and current strengths are almost the same for the corresponding butadiyne-bridged ZnP dimer. The current strength across the butadiyne linker is -3.3 nA/T as compared to -4.0 nA/T for the ethyne bridge. The butadiyne-bridged ZnP dimer has been synthesized by Tokuji *et al.* via a copper-catalyzed coupling reaction.[17] The number of π-electrons perpendicularly to the molecular plane of the inner ring is 14 for the ethyne-bridged system and 18 for the butadiyne-bridged one, whereas the overall number of available π-electrons is 56 and 60 for the two dimers, respectively.

We calculated the current strengths and current pathways for ethene-bridged and thiophene-bridged ZnP dimers, (**7**) and (**8**). Thiophene-bridged ZnP dimers and trimers have been synthesized by Song *et al.*[15,105] The net current strength across the linker bridges of the ethene-bridged and thiophene-bridged ZnP dimers is about 3.5-3.8 nA/T in the paratropic direction showing that the current strength across the bridge is almost independent of the chosen linker. The position where the linker is attached to the porphyrin is not very important either as illustrated by molecule (**9**). By attaching one of the butadiyne bridges to the other β position forming an inner ring that consists of 20 carbon atoms leads to a locally paratropic current of 1.9 nA/T across the bridge. Thus, the overall number of π-electrons is more important for the global current strength than the number of π-electrons around the inner ring.

We also studied asymmetric porphyrin dimers consisting of two different metal porphyrins. The current strengths along the linker of the ethyne- and butadiyne-bridged heterometallated dimers MgP-ZnP (**10**) and (**11**) are 4.1 and 3.1 nA/T in the paratropic direction, which are practically the same current strengths that we obtained for the corresponding ZnP dimers.

4.3 Free-Base and Zinc Isoporphyrin Dimers

The current densities and current strengths of ethyne-bridged dimers of ZnIP (**12**) and IP (**13**) were calculated. A streamline representation of the current density and the current pathway are illustrated in Fig. 5. The current pathway is not interrupted at the saturated meso-carbon atom, but a current strength of 9.9 nA/T passes the CH_2 moiety. In the ZnIP dimer, the outer protons are deshielded having chemical shifts of 7-8 ppm. The current flow splits at the pyrrole ring into an inner and outer route with current strengths of 3.2 nA/T and 7.3 nA/T, respectively. A local diatropic ring current of 1.1 nA/T flows around the Zn-N-C six-membered ring. The current along the outer route splits into a

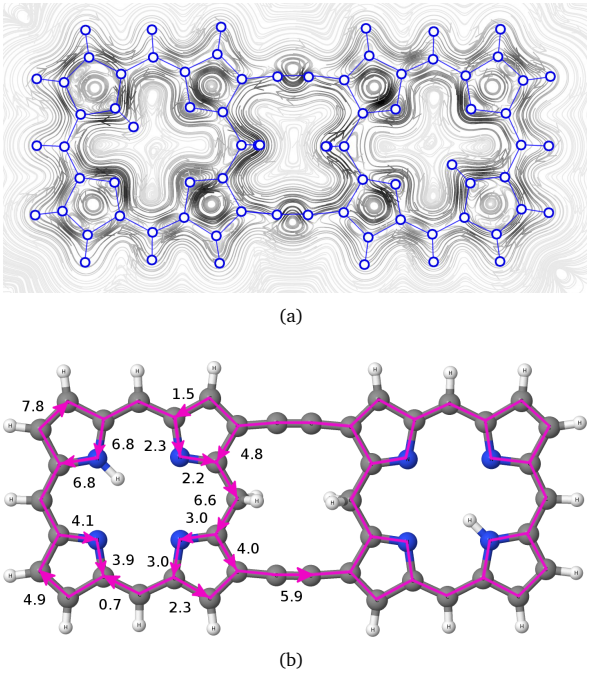

(a) (b)

Fig. 6 (a) Streamline plot of the calculated magnetically induced current densities calculated 1 bohr above the molecular plane of a ethyne-bridged IP dimer (**13**). (b) Calculated net current strengths passing selected bonds are given for an ethyne-bridged IP dimer (**13**). The current pathway is drawn in pink. A net paratropic current strength is found at the linker.

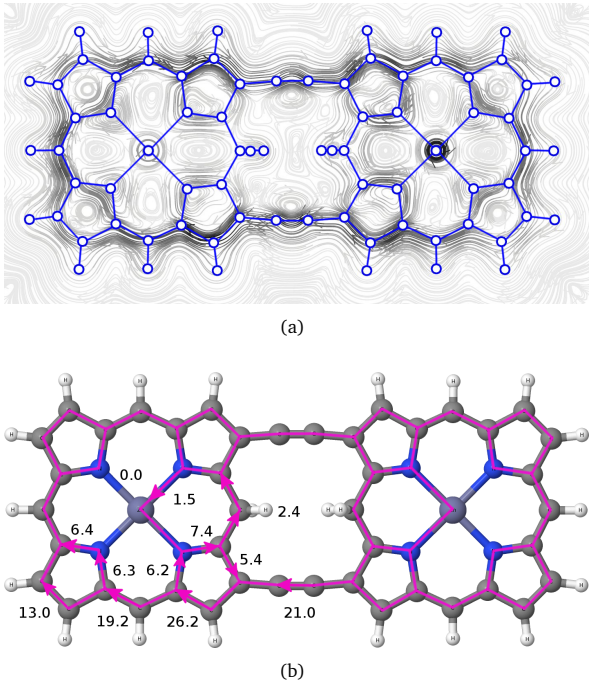

(a) (b)

Fig. 7 (a) Streamline plot of the calculated magnetically induced current density calculated 1 bohr above the molecular plane of the neutral ethyne-bridged ZnPS dimer with saturated meso carbons (**14**). (b) Calculated net current strengths passing selected bonds are given for the neutral ethyne-bridged ZnPS dimer with saturated meso carbons (**14**). The current pathway is drawn in pink. A strong net diatropic current strength passes the linker bridge.

current of 4.8 nA/T that passes the ethyne bridge in the paratropic direction and a current of 2.2 nA/T that continues around the isoporphyrin ring. The current passing the ethyne bridge is stronger than for the ZnP dimer and the ring current of the isoporphyrin ring is weaker. A ring current of 4.3 nA/T is sustained by the isoporphyrin ring. The two pyrrole rings without ethyne bridges sustain a local diatropic ring current of 2.7-2.9 nA/T.

For the ethyne-bridged IP dimer in Fig. 6, the strength of the current passing the linker is 5.9 nA/T in the paratropic direction, which is 1.1 nA/T stronger than for the ethyne-bridged ZnIP dimer. The global ring current around the IP rings is only 0.7 nA/T, whereas the pyrrole rings without the ethyne bridge sustain local ring currents of 3.9-4.1 nA/T and 6.8 nA/T, respectively. The strength of the current passing the CH_2 moiety is 6.6 nA/T, which splits into an outer and inner branch of 4.0 nA/T and 3.0 nA/T, respectively. The current along the outer route continues across the ethyne bridge, whereas the current in the inner branch splits into a small porphyrinoid ring current of 0.7 nA/T and the rest of 2.3 nA/T flows towards the ethyne bridge.

The IP rings are nonaromatic with two aromatic pyrrolic rings. The pyrrole ring with an inner hydrogen sustains a stronger local ring current than the one without the inner hydrogen. The inner ring between the two IP moieties is weakly antiaromatic sustaining a paratropic ring current of 5.9 nA/T that flows on both sides of the pyrrolic rings at the ethyne linker bridge. The number of available π-electrons is 52.

4.4 Zinc Porphyrin Dimers with Saturated Meso Carbons

Intermediates between the ZnP and ZnIP dimers having $(4n+2)$ π-electrons might be aromatic. Neutral ethyne- and butadiyne-bridged ZnPS dimers (**14**) and (**15**) are obtained by saturating the meso carbon of the ZnP dimers (**5**) and (**6**) by adding hydrogens. The obtained neutral ZnPS dimers have 54 and 58 π-electrons, respectively. A streamline plot of the current density and the current pathway of (**14**) are shown in Fig. 7.

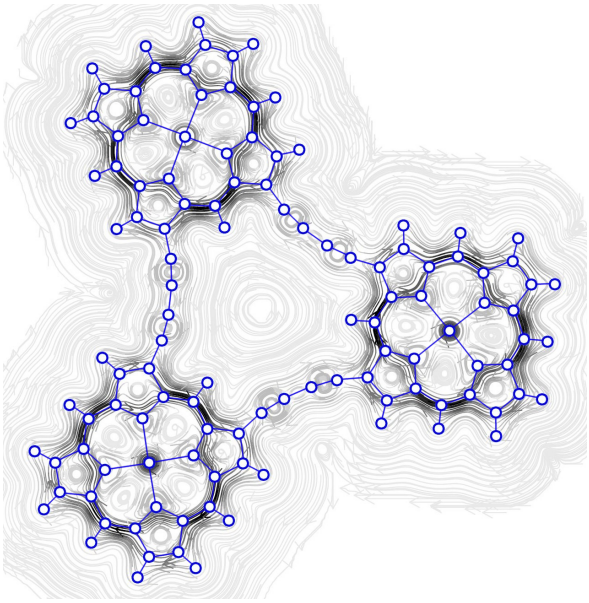

(a)

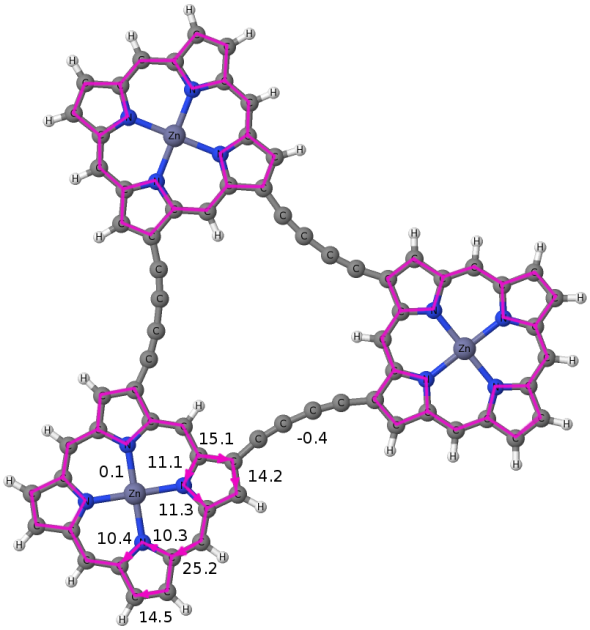

(b)

Fig. 8 (a) Streamline plot of the calculated magnetically induced current densities calculated 1 bohr above the molecular plane of butadiyne-bridged ZnP trimer (**16**). (b) Calculated net current strengths passing selected bonds are given for a butadiyne-bridged ZnP trimer (**16**). The current pathway is drawn in pink. The current pathway is cut at the linker. Due to the very small current strength at the linker, a global net current pathway is avoided. The porphyrin rings maintain a strong net diatropic current strength and the current strengths of the corresponding bonds are similar to the isolated monomer.

The calculations show that a strong net diatropic current strength of 21.0 nA/T passes the linker bridge and continues around the ZnIP moieties. Thus, a strong current arises when the number of electrons fulfills Hückels $(4n+2)$ rule. The pyrrole rings next to the bridge sustain a local diatropic ring current of 5.4 nA/T. The Zn-N-C six-membered ring sustains a weak local ring current of 1.5 nA/T. A weak current of 2.4 nA/T passes the saturated CH_2 moiety. The global ring current around the porphyrinoid is 19.2 nA/T, which splits at the pyrrole rings into 6.3-6.4 nA/T along the inner C-N bonds and 13.0 nA/T in the outer route.

The current pattern of the corresponding butadiyne-bridged ZnPS dimer is similar. The current strength across the butadiyne linker bridges is 19.8 nA/T or only 1.2 nA/T weaker than for the ethyne-bridged one. The global ring current around the porphyrinoids is 18.5 nA/T and 2.2 nA/T pass the saturated CH_2 group.

4.5 Zinc Porphyrin Trimers

A butadiyne-bridged ZnP trimer with aryl groups in meso position has been prepared and characterized by Tokuji *et al.*[17] We have calculated the current density of an unsubstituted ZnP trimer (**16**) to lower computational costs. The omitted aryl groups lead to 0.6-0.8 ppm higher chemical shifts of the β protons due to the missing mesomeric effect (-M), which also lowers the current strength, since electron density is pulled out of the porphyrin ring.[48]

A streamline representation of the current density and the current pathway of (**16**) are shown in Fig. 8. A weak net paratropic current strength of 0.4 nA/T passes the butadiyne linker. Thus, the inner ring formed by the porphyrins and the butadiyne bridges is nonaromatic. The current strength of the porphyrin moieties of 25.2 nA/T is close to the ring-current strength of 26.6 nA/T obtained for the isolated ZnP monomer. The current pathways of the individual ZnP moieties are very similar to the ones for the ZnP molecule. But the linker slightly increases the resistance leading to a larger current strength of 11.1-11.3 nA/T along the inner route as compared to 10.3-10.4 nA/T for the two other pyrrole rings of the ZnP moieties. The molecule has 90 π-electrons perpendicularly to the molecular plane fulfilling Hückel's rule for aromaticity. However, global aromaticity would also weaken the aromaticity of the individual ZnP rings. The conflict leads to a globally nonaromatic ZnP trimer with strongly aromatic ZnP units.

Similar calculations on the conjugated ZnP trimers show that neither the corresponding ethyne-bridged ZnP trimer (**17**) nor the ethyne-bridged ZnP trimer with bridges in different β positions (**18**) nor the ZnP trimer with two ethyne bridges in β positions and one butadiyne bridge in meso position (**19**) sustain a strong current strength at the linkers. The corresponding current strengths are 1.1 nA/T, 0.1 nA/T and -0.1 nA/T, respectively.

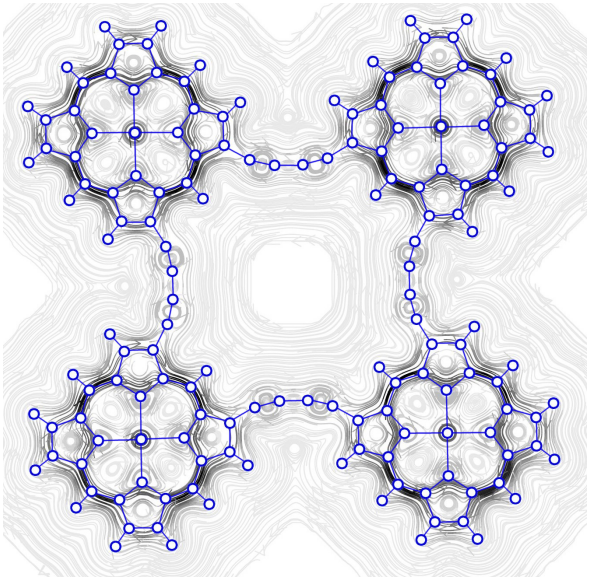

(a)

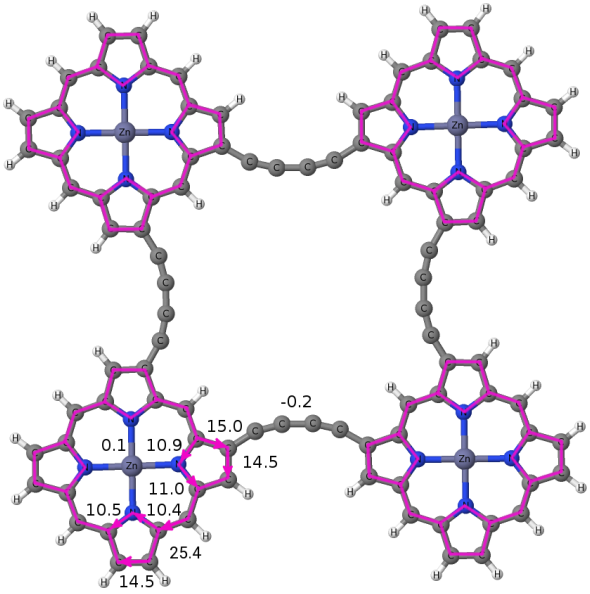

(b)

Fig. 9 (a) Streamline plot of the calculated magnetically induced current densities calculated 1 bohr above the molecular plane of a butadiyne-bridged ZnP tetramer (**20**). (b) Calculated net current strengths passing selected bonds are given for a butadiyne-bridged ZnP tetramer (**20**). The current pathway is drawn in pink. No net current flow is observed at the bridge.

4.6 Zinc Porphyrin Tetramers

A butadiyne-bridged ZnP tetramer (**20**) with 120 π-electrons has also been studied. A streamline plot of the current density and the current pathway are shown in Fig. 9. The net current strength passing the butadiyne bridges is only -0.2 nA/T. The current strengths in the porphyrin bond are very similar to the ones of the ZnP trimer and the isolated ZnP molecule. The ZnP rings sustain a net diatropic ring-current strength of 25.4 nA/T as compared to 26.6 nA/T for ZnP.

The current strength through the linker bridges of an ethyne-bridged ZnP tetramer (**21**) is 0.5 nA/T and the one for an all meso-to-meso butadiyne-bridged ZnP tetramer (**22**) is 0.9 nA/T. The inner ring in the three ZnP tetramers is nonaromatic, whereas the ZnP moieties remain as aromatic as independent ZnP molecules. The ZnP tetramers do not sustain any global ring-current.

4.7 Free-Base Isoporphyrin Tetramers

The β-to-β butadiyne-bridged IP tetramers (**23**) and meso-to-meso butadiyne-bridged IP tetramers have been studied. The corresponding ZnIP compounds have not been considered because they have a net charge of +4 as each ZnP moiety has a charge of +1. A streamline representation of the current density and the calculated current pathway are shown in Fig. 10. A current strength of 0.2 nA/T passing the butadiyne bridges is very small. The IP rings of the tetramer behave like the isolated monomer maintaining a current strength of 6.3 nA/T through the CH_2 group. The other current strengths are also similar to the ones obtained for a single IP molecule. The current strength of the bridge is also independent of the connecting position, as the current strength across the bridges of the meso-to-meso butadiyne-bridged IP tetramer (**24**) vanishes.

4.8 Zinc Porphyrin Tetramer with a Saturated Meso Carbon

The current strengths and pathways have been calculated for a butadiyne bridged ZnPS tetramer with 116 π electrons. The molecular structure and the strengths of the current pathways are shown in the ESI. The tetramer with $4n$ π electrons is weakly antiaromatic sustaining a global paratropic ring current of 5.7 nA/T. The aromaticity of the individual ZnPS units is destroyed by the saturated CH_2 moiety in the meso position making a global paratropic ring current feasible. A very weak paratropic ring current flows along the outer edge of the four ZnPS units and the individual pyrrole rings sustain diatropic ring currents of 6-7 nA/T, which is about half the ring-current strength of pyrrole.[103] The main part of the global paratropic ring current takes the innermost route at the ZnPS units, which also destroys the aromaticity of the corresponding pyrrole ring.

5 Summary and Conclusion

Magnetically induced current densities have been calculated and analyzed for a number of cyclic porphyrin and isoporphyrin arrays by performing calculations at the DFT/B3LYP level using TUR-

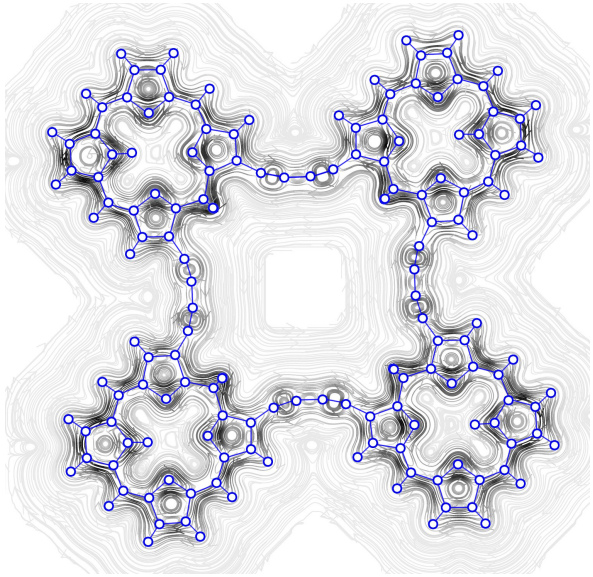

(a)

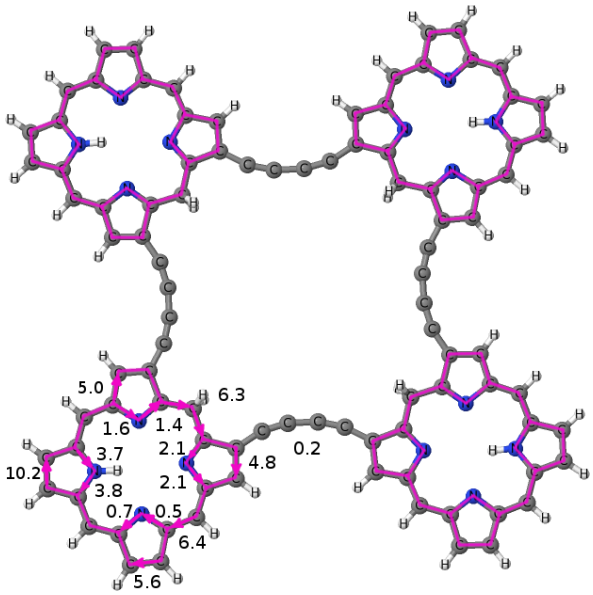

(b)

Fig. 10 (a) Streamline plot of the calculated magnetically induced current densities calculated 1 bohr above the molecular plane of a butadiyne-bridged IP tetramer (**23**). (b) Calculated net current strengths passing selected bonds are given for a butadiyne-bridged IP tetramer (**23**). The current pathway is drawn in pink. No global net current flow exists.

BOMOLE and the gauge-including magnetically induced current (GIMIC) method. The small deviations from Kirchoff's law are due to the use of a comparably small basis set (def2-SVP) and due to inaccuracies in the numerical integration. The studied free-base and zinc isoporphyrin monomers possess net diatropic current strengths of 6.7 and 10.1 nA/T, respectively, as compared with the corresponding porphyrins that sustain a current strength of 27.2[42] and 26.6 nA/T. Despite the interrupted conjugated system, isoporphyrins are at least to some extent aromatic according to the ring-current criterion. All available π-electrons participate in the ring current that splits at the pyrrole rings into an inner and an outer route. The outer pathway is the preferred one sustaining about 80% of the global ring current of ZnIP. IP and ZnIP sustain local ring currents in the pyrrole ring with an inner hydrogen and in the Zn-N-C six-membered ring, respectively.

The porphyrin and isoporphyrin dimers sustain net paratropic ring currents of 1.9-5.9 nA/T passing the ethyne or the butadiyne bridges. Thus, the inner ring formed by the porphyrinoids and the linker bridges can be considered weakly antiaromatic. The greater current strength of the isoporphyrin systems is due to the weaker ring current of the isoporphyrin rings as compared to the porphyrin ones. Inside the inner ring reigns a paratropic current, while a weaker diatropic current flows outside the ring. The current pathway of zinc(II) isoporphyrin is more complex due to radial current pathways involving zinc. Intermediate neutral zinc porphyrinoid compounds containing a saturated meso-carbon group possess a strong net diatropic current strength of 19.8-21.0 nA/T. Hence, the compounds are aromatic. Due to the saturated meso carbons, the ring current flows around the outer edge of the whole molecule involving all π-electrons. The strong ring current are in line with Hückels $(4n+2)$ aromaticity rule taking all π-electrons into account.

According to Hückel's rule, a diatropic global ring current is expected for the porphyrinoid trimer, whereas the tetramers with $4n$ π electrons should sustain a global paratropic ring current. In fact, for none of the larger porphyrin and isoporphyrin arrays, a significant ring current passes the linker. Instead, the porphyrinoid monomers sustain strong local diatropic ring currents that are very similar to the ones for the corresponding monomers, indicating a competition between the aromaticity of the individual porphyrinoids and the aromaticity of the whole molecule.

None of the trimers sustains a significant current strength at the linker bridge, even though the butadiyne-bridged zinc(II) porphyrin trimer with 90 π-electrons fulfills Hückel's aromaticity rule. The studied porphyrin and isoporphyrin tetramers contain 4n π-electrons. Hence, the molecules sustain the diatropic ring currents around the individual porphyrinoid rings. The current strengths are very similar to the ones of the corresponding monomers. The trimers and tetramers do not sustain any global ring current due to the competition between the aromaticity of the individual porphyrinoids and the whole system. The saturated meso carbons of the studied ZnPS tetramer largely stop the current flow along the outer edge of the ZnPS units. The ZnPS

tetramer with $4n$ π electrons is weakly antiaromatic sustaining a global paratropic ring current of 5.7 nA/T that passes only the innermost pyrrolic moiety of the ZnPS units.

Overall, current density calculations turned out to be a useful tool for quantifying the aromatic properties of porphyrin oligomers from current pathways as well as from current strengths passing selected chemical bonds. Like chemical shieldings, these quantities are available from the calculated magnetic response, but they are much more directly related to aromaticity and thus provide respective information with much higher reliability.

6 Acknowledgments

Y.J.F. acknowledges support from Studienstiftung des deutschen Volkes (German Academic Scholarship Foundation) including support for his research stay at the University of Helsinki. This work was supported by The Academy of Finland through project 275845. The authors wish to acknowledge CSC – IT Center for Science, Finland for computational resources. We thank Isaac Benkyi for discussions.

References

1 *The Porphyrin Handbook*, ed. K. M. Kadish, K. M. Smith and R. Guilard, Academic Press, San Diego, 1999, vol. 1-10.

2 *The Porphyrin Handbook*, ed. K. M. Kadish, K. M. Smith and R. Guilard, Academic Press, San Diego, 2003, vol. 11-20.

3 *Handbook of Porphyrin Science*, ed. K. M. Kadish, K. M. Smith and R. Guilard, World Scientific Publishing, Singapore, 2010, vol. 1-10.

4 *Handbook of Porphyrin Science*, ed. K. M. Kadish, K. M. Smith and R. Guilard, World Scientific Publishing, Singapore, 2011, vol. 11-15.

5 *Handbook of Porphyrin Science*, ed. K. M. Kadish, K. M. Smith and R. Guilard, World Scientific Publishing, Singapore, 2012, vol. 16-25.

6 *Handbook of Porphyrin Science*, ed. K. M. Kadish, K. M. Smith and R. Guilard, World Scientific Publishing, Singapore, 2013, vol. 26-30.

7 *Handbook of Porphyrin Science*, ed. K. M. Kadish, K. M. Smith and R. Guilard, World Scientific Publishing, Singapore, 2014, vol. 31-35.

8 *Handbook of Porphyrin Science*, ed. K. M. Kadish, K. M. Smith and R. Guilard, World Scientific Publishing, Singapore, 2016, vol. 36-44.

9 H. L. Anderson, *Chem. Commun.*, 1999, 2323–2330.

10 J. R. Reimers, N. S. Hush and M. J. Crossley, *J. Porphyrins Phthalocyanines*, 2002, **6**, 795–805.

11 G. de la Torre, G. Bottari, M. Sekita, A. Hausmann, D. M. Guldi and T. Torres, *Chem. Soc. Rev.*, 2013, **42**, 8049–8105.

12 H. Huang, W. Song, J. Rieffel and J. F. Lovell, *Front. Phys.*, 2015, **3**, 23.

13 T. Tanaka and A. Osuka, *Chem. Soc. Rev.*, 2015, **44**, 943–969.

14 K. Sugiura, Y. Fujimoto and Y. Sakata, *Chem. Commun.*, 2000, 1105–1106.

15 J. Song, S. Y. Jang, S. Yamaguchi, J. Sankar, S. Hiroto, N. Aratani, J.-Y. Shin, S. Easwaramoorthi, K. Kim, D. Kim, H. Shinokubo and A. Osuka, *Angew. Chem., Int. Ed.*, 2008, **47**, 6004–6007.

16 I. Hisaki, S. Hiroto, K. Kim, S. Noh, D. Kim, H. Shinokubo and A. Osuka, *Angew. Chem., Int. Ed.*, 2007, **46**, 5125–5128.

17 S. Tokuji, H. Yorimitsu and A. Osuka, *Angew. Chem., Int. Ed.*, 2012, **51**, 12357–12361.

18 D. Dolphin, R. H. Felton, D. C. Borg and J. Fajer, *J. Am. Chem. Soc.*, 1970, **92**, 743–745.

19 G. L. Closs and L. E. Closs, *J. Am. Chem. Soc.*, 1963, **85**, 818–819.

20 H. Xie and K. M. Smith, *Tetrahedron Lett.*, 1992, **33**, 1197–1200.

21 K. M. Barkigia, M. W. Renner, H. Xie, K. M. Smith and J. Fajer, *J. Am. Chem. Soc.*, 1993, **115**, 7894–7895.

22 W. R. Fawcett, M. Fedurco, K. M. Smith and H. Xie, *J. Electroanal. Chem.*, 1993, **354**, 281–287.

23 J. P. Evans, F. Niemevz, G. Buldain and P. O. de Montellano, *J. Biol. Chem.*, 2008, **283**, 19530–19539.

24 I. Garcia-Bosch, S. K. Sharma and K. D. Karlin, *J. Am. Chem. Soc.*, 2013, **135**, 16248–16251.

25 H. Xie, S. H. Leung and K. M. Smith, *J. Porphyrins Phthalocyanines*, 2002, **06**, 607–616.

26 C. Mwakwari, F. R. Fronczek and K. M. Smith, *Chem. Commun.*, 2007, 2258–2260.

27 J. Bhuyan and S. Sarkar, *Chem. Eur. J.*, 2010, **16**, 10649–10652.

28 Z. Cong, T. Kurahashi and H. Fujii, *J. Am. Chem. Soc.*, 2012, **134**, 4469–4472.

29 J. Bhuyan, *Dalton Trans.*, 2016, **45**, 2694–2699.

30 P. Schweyen, M. Hoffmann, J. Krumsieck, B. Wolfram, X. Xie and M. Bröring, *Angew. Chem., Int. Ed.*, 2016, **55**, 10118–10121.

31 J. Bhuyan, *Dalton Trans.*, 2015, **44**, 15742–15756.

32 E. Hückel, *Z. Physik*, 1931, **70**, 204–286.

33 E. Hückel, *Z. Physik*, 1931, **72**, 310–337.

34 E. Hückel, *Z. Physik*, 1932, **76**, 628–648.

35 E. Hückel, *Grundzüge der Theorie ungesättigter und aromatischen Verbindungen*, Verlag Chemie, Berlin, 1938, pp. 71–85.

36 J. Jusélius, D. Sundholm and J. Gauss, *J. Chem. Phys.*, 2004, **121**, 3952–3963.

37 S. Taubert, D. Sundholm and J. Jusélius, *J. Chem. Phys.*,

2011, **134**, 054123.
38 H. Fliegl, S. Taubert, O. Lehtonen and D. Sundholm, *Phys. Chem. Chem. Phys.*, 2011, **13**, 20500–20518.
39 D. Sundholm, H. Fliegl and R. J. F. Berger, *WIREs Comput Mol Sci*, 2016, **6**, 639–678.
40 H. Fliegl, D. Sundholm, S. Taubert and F. Pichierri, *J. Chem. Phys. A*, 2010, **114**, 7153–7161.
41 H. Fliegl, D. Sundholm and F. Pichierri, *Phys. Chem. Chem. Phys.*, 2011, **13**, 20659–20665.
42 H. Fliegl and D. Sundholm, *J. Org. Chem.*, 2012, **77**, 3408–3414.
43 H. Fliegl, N. Özcan, R. Mera-Adasme, F. Pichierri, J. Jusélius and D. Sundholm, *Mol. Phys.*, 2013, **111**, 1364–1372.
44 R. R. Valiev, H. Fliegl and D. Sundholm, *J. Phys. Chem. A*, 2013, **117**, 9062–9068.
45 R. R. Valiev, H. Fliegl and D. Sundholm, *Phys. Chem. Chem. hys.*, 2014, **16**, 11010–11016.
46 R. R. Valiev, H. Fliegl and D. Sundholm, *Phys. Chem. Chem. Phys.*, 2015, **17**, 14215–14222.
47 R. R. Valiev, H. Fliegl and D. Sundholm, *J. Phys. Chem. A*, 2015, **119**, 1201–1207.
48 H. Fliegl, F. Pichierri and D. Sundholm, *J. Phys. Chem. A*, 2015, **119**, 2344–2350.
49 I. Benkyi, H. Fliegl, R. R. Valiev and D. Sundholm, *Phys. Chem. Chem. Phys.*, 2016, **18**, 11932–11941.
50 I. Morao, B. Lecea and F. P. Cossío, *J. Org. Chem.*, 1997, **62**, 7033–7036.
51 J. Jusélius and D. Sundholm, *Phys. Chem. Chem. Phys.*, 1999, **1**, 3429–3435.
52 P. Lazzeretti, *Progr. NMR Spectr.*, 2000, **36**, 1–88.
53 P. Lazzeretti, *Phys. Chem. Chem. Phys.*, 2004, **6**, 217–223.
54 S. Pelloni, G. Monaco, P. Lazzeretti and R. Zanasi, *Phys. Chem. Chem. Phys.*, 2011, **13**, 20666–20672.
55 S. Pelloni and P. Lazzeretti, *J. Phys. Chem. A*, 2013, **117**, 9083–9092.
56 Z. Badri, S. Pathak, H. Fliegl, P. Rashidi-Ranjbar, R. Bast, R. Marek, C. Foroutan-Nejad and K. Ruud, *J. Chem. Theory Comput.*, 2013, **9**, 4789–4796.
57 G. Monaco and R. Zanasi, *J. Phys. Chem. A*, 2014, **118**, 1673–1683.
58 C. Foroutan-Nejad, *Theoret. Chim. Acta*, 2015, **134**, 8.
59 D. Du, D. Sundholm and H. Fliegl, *J. Chin. Chem. Soc.*, 2016, **63**, 93–100.
60 H. Fliegl, J. Jusélius and D. Sundholm, *J. Phys. Chem. A*, 2016, **120**, 5658–5664.
61 A. D. Becke, *J. Chem. Phys.*, 1993, **98**, 5648–5652.
62 C. Lee, W. Yang and R. G. Parr, *Phys. Rev. B*, 1988, **37**, 785–789.
63 R. Ahlrichs, M. Bär, M. Häser, H. Horn and C. Kölmel, *Chem. Phys. Lett.*, 1989, **162**, 165–169.
64 F. Furche, R. Ahlrichs, C. Hättig, W. Klopper, M. Sierka and F. Weigend, *WIREs Comput Mol Sci*, 2014, **4**, 91–100.
65 *TURBOMOLE V7.0 2015 and V7.1 2016, a development of University of Karlsruhe and Forschungszentrum Karlsruhe GmbH, 1989-2007, TURBOMOLE GmbH, since 2007; available from http://www.turbomole.com*.
66 A. Schäfer, H. Horn and R. Ahlrichs, *J. Chem. Phys.*, 1992, **97**, 2571–2577.
67 F. Weigend and R. Ahlrichs, *Phys. Chem. Chem. Phys.*, 2005, **7**, 3297–3305.
68 M. Häser, R. Ahlrichs, H. P. Baron, P. Weis and H. Horn, *Theoret. Chim. Acta*, 1992, **83**, 455.
69 M. Kollwitz and J. Gauss, *Chem. Phys. Lett.*, 1996, **260**, 639–646.
70 M. Kollwitz, M. Häser and J. Gauss, *J. Chem. Phys.*, 1998, **108**, 8295–8301.
71 S. Grimme, J. Antony, S. Ehrlich and H. Krieg, *J. Chem. Phys.*, 2010, **132**, 154104.
72 *Jmol Version 14.0.13: an open-source Java viewer for chemical structures in 3D, http://www.jmol.org*.
73 *GIMP Version 2.8.16: GNU Image Manipulation Program, http://www.gimp.org*.
74 F. H. Allen, O. Kennard, D. G. Watson, L. Brammer, A. G. Orpen and R. Taylor, *J. Chem. Soc., Perkin Trans. 2*, 1987, S1–S19.
75 C. B. Storm and Y. Teklu, *J. Am. Chem. Soc.*, 1972, **94**, 1745–1747.
76 M. J. Crossley, L. D. Field, M. M. Harding and S. Sternhell, *J. Am. Chem. Soc.*, 1987, **109**, 2335–2341.
77 M. J. Crossley, M. M. Harding and S. Sternhell, *J. Org. Chem.*, 1992, **57**, 1833–1837.
78 J. Braun, M. Köcher, M. Schlabach, B. Wehrle, H. Limbach and E. Vogel, *J. Am. Chem. Soc.*, 1994, **116**, 6593–6604.
79 J. Braun, C. Hasenfratz, R. Schwesinger and H.-H. Limbach, *Angew. Chem., Int. Ed.*, 1994, **33**, 2215–2217.
80 J. Braun, H.-H. Limbach, P. G. Williams, H. Morimoto and D. E. Wemmer, *J. Am. Chem. Soc.*, 1996, **118**, 7231–7232.
81 L. Kümmerl, H. Kliesch, D. Wöhrle and D. Haarer, *Chem. Phys. Lett.*, 1994, **227**, 337–342.
82 J. R. Reimers, T. X. Lü, M. J. Crossley and N. S. Hush, *J. Am. Chem. Soc.*, 1995, **117**, 2855–2861.
83 A. Ghosh and J. Almlöf, *J. Phys. Chem.*, 1995, **99**, 1073–1075.
84 T. Vangberg and A. Ghosh, *J. Phys. Chem. B*, 1997, **101**, 1496–1497.
85 J. Baker, P. M. Kozlowski, A. A. Jarzecki and P. Pulay, *Theor.*

Chem. Acta., 1997, **97**, 59–66.
86 D. Sundholm, H. Konschin and M. Häser, *Chem. Eur. J.*, 1999, **5**, 267–273.
87 W. von E. Doering and F. L. Detert, *J. Am. Chem. Soc.*, 1951, **73**, 876–877.
88 A. Balaban, P. von Ragué Schleyer and H. S. Rzepa, *Chem. Rev.*, 2005, **105**, 3436–3447.
89 S. Taubert, J. Jusélius, D. Sundholm, W. Klopper and H. Fliegl, *J. Phys. Chem. A*, 2008, **112**, 13584–13592.
90 E. Steiner and P. W. Fowler, *J. Phys. Chem. A*, 2001, **105**, 9553–9562.
91 E. Steiner and P. W. Fowler, *ChemPhysChem*, 2002, **3**, 114–116.
92 P. W. Fowler and A. Soncini, *Polycyclic Aromatic Compounds*, 2004, **24**, 353–366.
93 H. S. Rzepa, *Chem. Rev.*, 2005, **105**, 3697–3715.
94 M. Bühl and A. Hirsch, *Chem. Rev.*, 2001, **101**, 1153–1183.
95 R. Herges, *Chem. Rev.*, 2006, **106**, 4820–4842.
96 M Stępień and L Latos-Grażyński and N Sprutta and P Chwalisz and L Szterenberg, *Angew. Chem. Int. Ed.*, 2007, **46**, 7869–7873.
97 S. Saito, J. Y. Shin, J. M. Lim, K. S. Kim, D. Kim and A. Osuka, *Angew. Chem. Int. Ed.*, 2008, **47**, 9657–9660.
98 N. Jux, *Angew. Chem. Int. Ed.*, 2008, **47**, 2543–2546.
99 S. M. Rappaport and H. S. Rzepa, *J. Am. Chem. Soc.*, 2008, **130**, 7613–7619.
100 S. Taubert, D. Sundholm and F. Pichierri, *J. Org. Chem.*, 2009, **74**, 6495–6502.
101 J. Jusélius and D. Sundholm, *Phys. Chem. Chem. Phys.*, 2008, **10**, 6630–6634.
102 D. Sundholm, R. J. F. Berger and H. Fliegl, *Phys. Chem. Chem. Phys.*, 2016, **18**, 15934–15942.
103 M. P. Johansson and J. Jusélius, *Lett. Org. Chem.*, 2005, **2**, 469–474.
104 H. Fliegl, D. Sundholm, S. Taubert, J. Jusélius and W. Klopper, *J. Phys. Chem. A*, 2009, **113**, 8668–8676.
105 J. Song, N. Aratani, H. Shinokubo and A. Osuka, *Chem. Sci.*, 2011, **2**, 748–751.

Table of content graphics

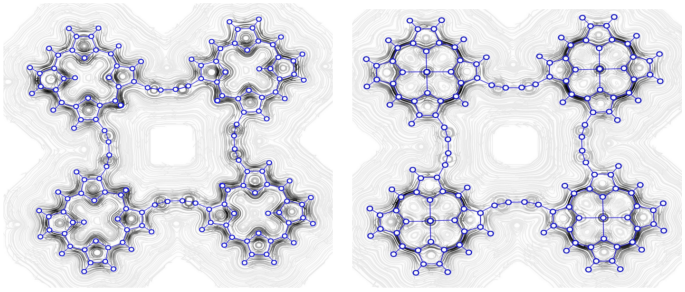

The aromaticity of cyclic porphyrin and isoporphyrin arrays has been studied by calculating the strength and pathways of magnetically induced current densities.